Synthetic microseismic datasets

Joe Wong and Peter M. Manning

ABSTRACT

We designed and created synthetic microseismic datasets for testing the accuracy of different source location algorithms. Three–component microseismograms with sources and receivers embedded in horizontally layered velocity structures were generated either by ray-tracing (RT) and convolution, or by 2D finite-difference (FD) modeling. The RT-modeled seismograms include direct and head-wave arrivals, but no reflected arrivals. The ray-tracing method can approximate some effects of TTI anisotropy in the layers. Traces from FD modeling include reflected as well as direct and head wave arrivals, but they do not include effects due to anisotropy. Gaussian noise and harmonic noise are added to the synthetic microseismograms to simulate different signal-to-noise levels, and the modeled data are stored in SEG2 format to conform to field-recorded data files.

INTRODUCTION

Although passive monitoring of microseismic events induced by hydraulic fracturing has been used for many years, the fundamental problem of locating hypocenters is still plagued by inaccuracies. Different algorithms and processing flows applied to the same dataset often produce radically different estimates of source locations. This is especially true if the acquisition aperture of the recording array is small in angular extent and if the microseismic arrivals are weak compared to the noise.

We have created synthetic microseismic datasets designed for testing different location algorithms such as migration (Chambers et al., 2008), inversion (Wong, 2009; Wong et al., 2010), and back-propagation (Han et al, 2010). Since the hypocenter coordinates for the synthetic data are known, the effectiveness and accuracy of different location methods can be evaluated for various recording geometries and noise levels.

The datasets consist of seismic traces obtained by ray-tracing or finite difference modeling of subsurface sources and receiver arrays. The P and S velocity structures are discrete layers with horizontal boundaries, and simulate geological structures that are common in many hydraulic fracture projects. Gaussian noise and harmonic noise are added to the synthetic traces to simulate microseismograms different signal-to-noise levels. The modeled data are stored in files with SEG2 format so that they are consistent with field-recorded data files.

Hypocenter location techniques require accurate relative amplitudes of the x, y, and z components of P wave arrivals in order that the direction cosines of the propagation vector at receivers may be estimated. They also require accurate arrival times of the P and/or S arrival times relative to some reference time that is not the actual time of occurrence t_0 of the associated microseismic event. Our modeling schemes do not yield true absolute amplitudes for the arrivals present on synthetic traces, but the relative amplitudes of the direct P-wave arrivals on a given 3C geophone are accurate, as are the arrival time moveouts of all modes.

VELOCIY-DENSITY MODEL

Figure 1 is a diagram depicting a horizontally-layered model used for ray-trace modeling. P-wave velocity, S-wave velocity, and relative density for each layer are shown. The model was constructed based on information provided by Devon personnel in Houston, and is a representation of geological structure typically encountered by hydraulic fracturing projects in the Barnett shale in Texas. The tops of the shale layers are located at depths of 1851 m, 2290 m, and 2365 m. The lower Barnett shale at 2365 m is a gas shale that is a target of hydraulic fracturing stimulation. The parameters of the model are listed on Table 1.

For the moment, we will assume that all the properties in each layer of this model are homogeneous and isotropic. In a later section of this report, we will indicate how ray tracing can be done if we assume TTI anisotropy within the shale layers.

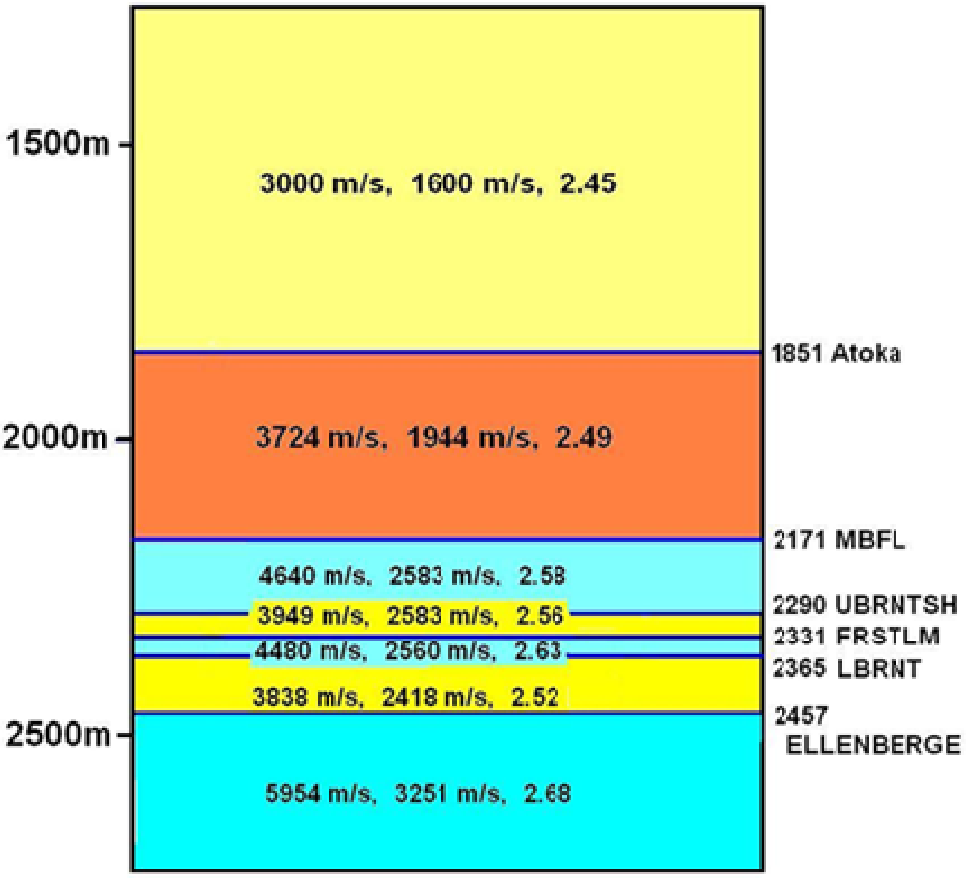

FIG. 1. Velocity-density model for calculating synthetic microseismic files by ray tracing.

Table 1. Velocity-density model for calculating microseismic data files using ray tracing. A visual representation of the model is shown on Figure 1.

Layer Number	Top of Layer (m)	P velocity (m/s)	S velocity (m/s)	ρ (gm/cc)
1	1500	3000	1600	2.30
2	1851	3724	1944	2.45
3	2171	4640	2583	2.49
4	2290	3949	2399	2.58
5	2331	4480	2560	2.63
6	2365	3838	2418	2.52
7	2457	5854	3251	2.68
8	3000	5854	3251	2.68

SOURCE-RECEIVER GEOMETRY

Arrays of three-component geophones array can be placed in one or more observation well located in 3D view of the acquisition geometry (Figure 2). The wells may be vertical, slanted or have horizontal sections. Microseismic sources can be placed at any depth and distance from the observation wells. The number of geophones in the arrays and the spacing between the geophones in the arrays can be varied. For this report, examples will be shown for a single vertical array with 16 or 24 geophones spaced at intervals of 25m.

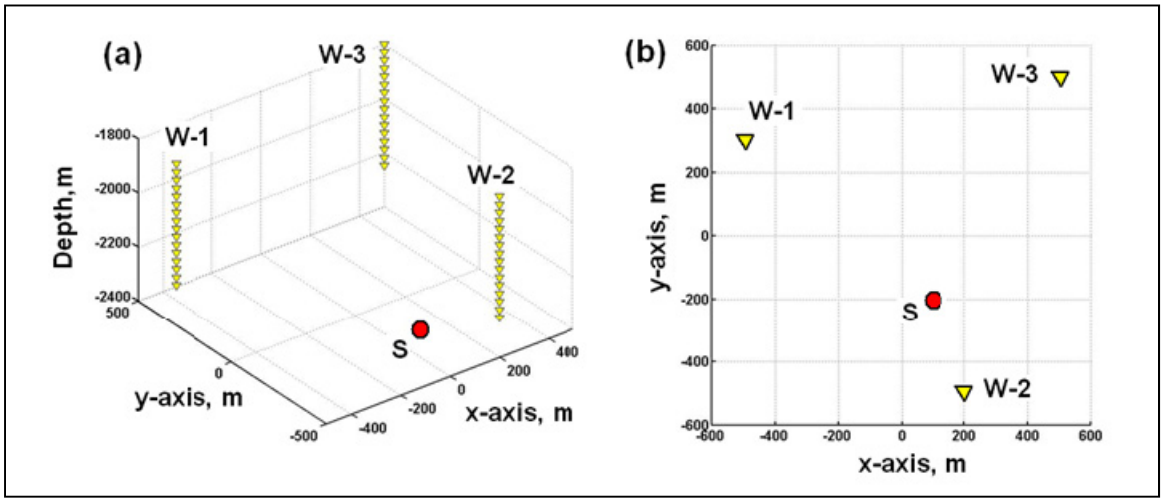

FIG. 2. Three observation wells surrounding a microseismic source S: (a) 3D view; (b) plan view.

SEISMOGRAMS PRODUCED BY RAY-TRACING

Ray-tracing using Snell's Law at layer interfaces give P- and S-wave refracted raypaths between the source and each receiver as well as the travel times and incident directions. Appropriate wavelets approximately scaled for geometric spreading are initiated at the appropriate arrival times. Three-component traces with amplitudes in the correct proportions for each receiver are calculated for the P-wave arrivals by applying the direction cosines of the incident P-wave raypath at each receiver position. Both the P and S wavelets have the form

$$s(t) = A_0 * \sin(2\pi f t) * \exp(-\kappa t)\,. \qquad (1)$$

The parameters f and k are arbitrary; in synthesizing our microseismograms, we have chosen f = 300 Hz, κ = 80/s for the P arrivals, and f = 200 Hz, κ = 50/s for the S arrivals.

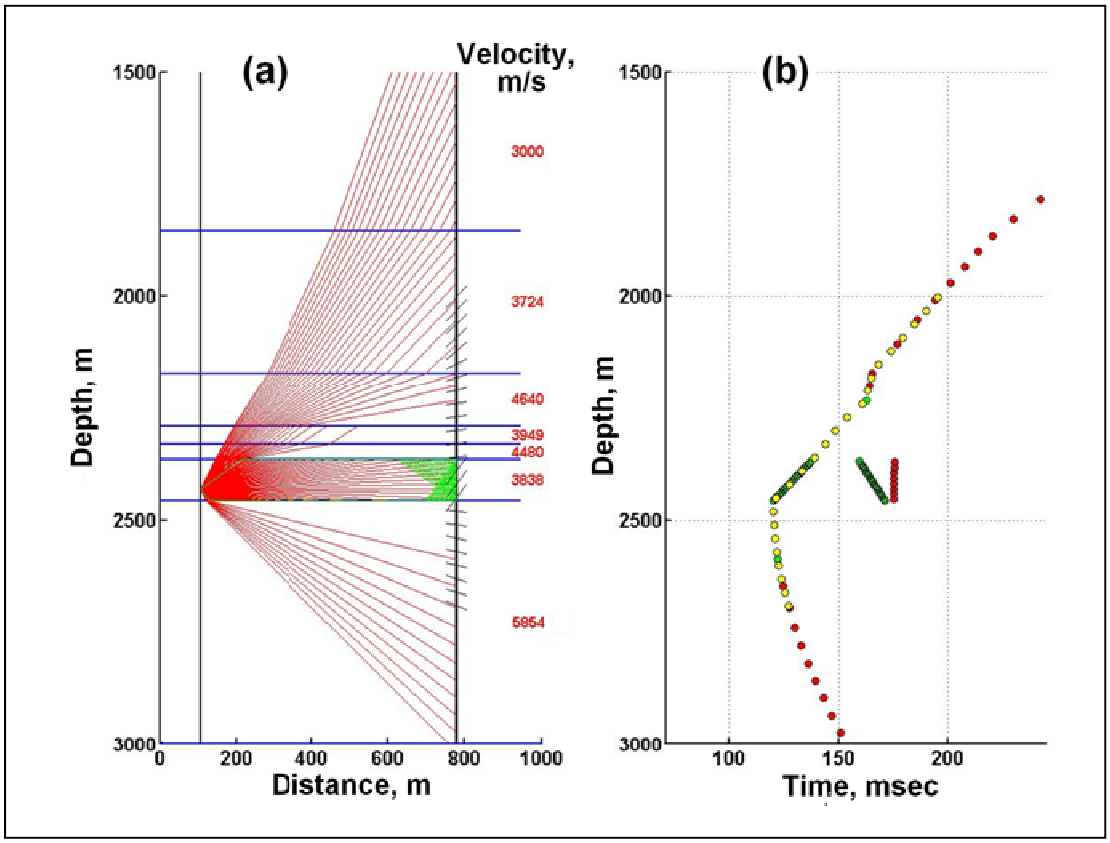

FIG. 3. Rays traced through the velocity model of Figure 1, with associated first arrival times. Head-wave rays are shown in green; direct-arrival rays are shown in red. The microseismic source coordinates are (x_s, y_s, z_s) = (100 m, -200 m, 2425 m). The receiver coordinates are (x_r, y_r, z_r) = (500 m, 500 m, 2000 to 2575 m), with spacing Δz = 25 m. They are associated with well W-3 on Figure 2.

An example of ray tracing is displayed on Figure 3. Figure 3(a) shows a network of P-wave rays traced from a source location in the well on the left to receiver positions in the observation well on the right. The horizontal scale is distance across the 2D plane spanned by the two wells. Figure 3(b) shows the arrival times for the P-wave. P-wave

arrival times for 24 geophones (positions indicated by the short slanted lines on the observation well) are obtained by interpolation of arrivals found for a dense network of traced rays. The propagation directions of the first P-wave arrivals at the geophones are indicted by the short slanted lines on the observation well. A similar figure showing the network of traced S wave arrivals can also be drawn.

This ray-tracing method produces seismograms that show only head-wave arrivals and direct arrivals; for simplicity, we have chosen not to include reflected or guided wave arrivals. The 3C amplitudes for each P-wave arrival are made to conform to the proper values demanded by the incident propagation direction at each receiver. However, the relative amplitudes on the modeled seismograms between different modes (P and S arrivals, and head waves) are arbitrary and have no significance.

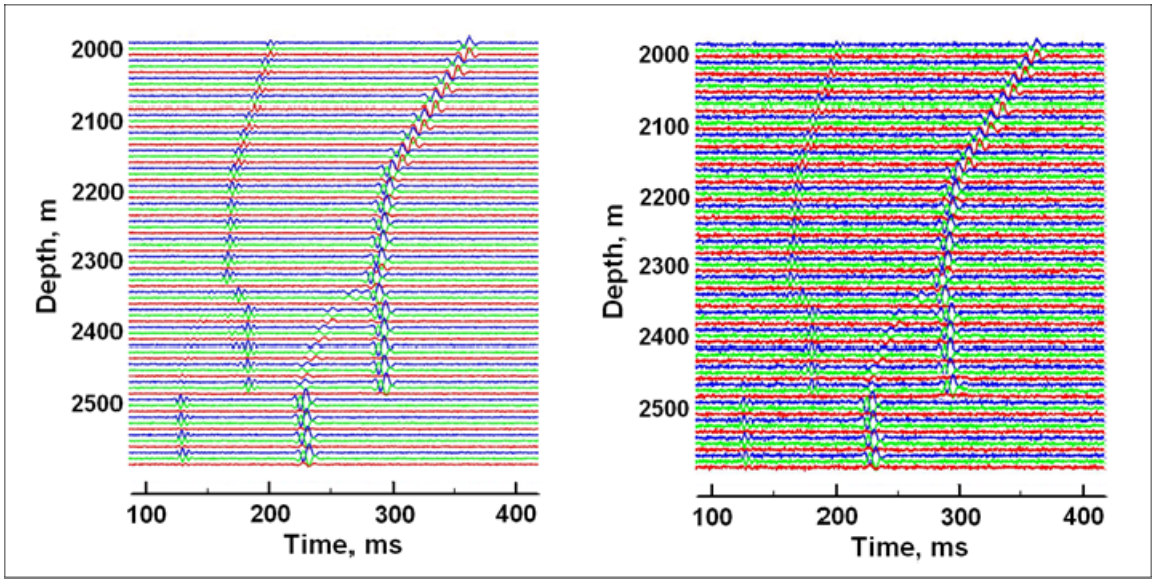

FIG. 4. Synthetic microseismograms produced by ray tracing and convolution. The 3C seismograms for each geophone are plot as a triplet of x (in blue), y (in green), and z (in red) components. Gaussian noise has been added to the clean traces on the left to obtain the noisy traces on the right.

Figure 4 shows gathers of 3C seismograms for the source location and geophone positions for well W-3 on Figure 2. The amplitudes of the P arrivals have been set to 0.5 times the amplitudes of the S arrivals. The head wave amplitudes have been arbitrarily set to 0.25 times the direct arrival amplitudes. The SNR values are set relative to the direct P wave amplitudes. The clean traces have SNR = 10, while the noisy traces have SNR = 3. The higher noise levels for the gather on the right completely obscure the weak head wave P arrivals.

RAY TRACING THROUGH ANISOTROPIC LAYERS

Wong (2010) has used an approximation developed by Byun et al. (1989) and Kumar et al. (2004) to devise a procedure for tracing quasi-P (qP) rays through horizontal velocity layers with TTI. The Byun/Kumar approximation for quasi-P wave group velocities is given by:

$$V_p^{-2}(\emptyset) = a_0 + a_1 \cos^2\emptyset - a_2 \cos^4\emptyset \ , \quad (1)$$

$$a_0 = V_h^{-2} \ , \quad (2)$$

$$a_1 = 4V_{45}^{-2} - 3V_h^{-2} - V_v^{-2} \ , \quad (3)$$

$$a_2 = 4V_{45}^{-2} - 2V_h^{-2} - 2V_v^{-2} \ , \quad (4)$$

where V_v, V_h, and V_{45} are the group velocities in the vertical (∅=0°), horizontal (∅=90°), and 45° dip angle directions. The VTI symmetry axis can be tilted to simulate TTI (Kumar et al. 2004; Wong, 2010). For the isotropic case, a_1 and a_1 are identically zero.

Figure 5 shows an example of synthetic P arrivals obtained when the low velocity layer between 2400 m and 2600 m has its VTI symmetry axis tilted clockwise by 30º. Figure 5(a) shows the raypaths traced from a source on left to an array of receivers on the right. On Figure 5(b), the red curve represents the arrival times if all layers have isotropic velocity values as shown. The small red dots are the arrival times when the layer just below 2400 m is TTI. Even though there is only a single TTI layer, there is significant deviation of the TTI arrival times from the isotropic times. Clearly, the effects of anisotropy must be taken into account if one were to use the arrival times to locate a microseismic hypocenter.

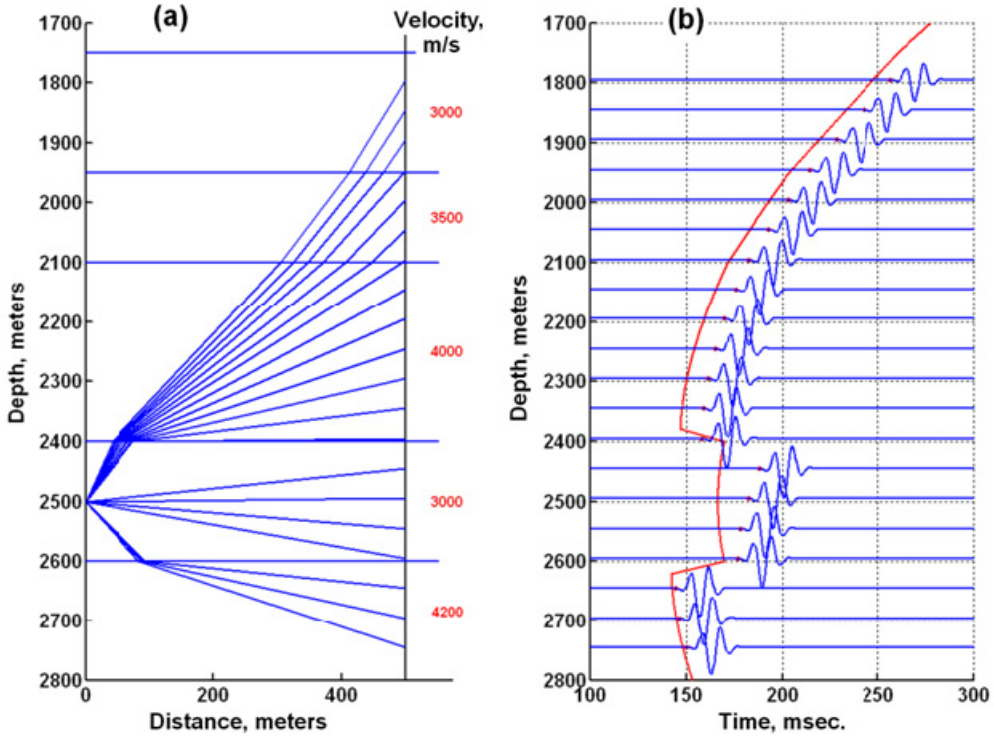

FIG. 5. Example of ray tracing through one TTI layer located at depths between 2400 m and 2600 m. The parameters used in Equations 1 to 4 to trace the raypaths and determine the arrival times are with V_h =3000 m/s, V_v =2400 m/s, and V_{45} = 2585 m/s.

Before we include anisotropy in our ray tracing scheme for generating synthetic microseismic data files, we must first develop formulae similar to Equations 1 to 6 for the quasi-shear group velocities qV_{sv} and qV_{sh}.

SEISMOGRAMS PRODUCED BY 2D FINITE DIFFERENCE CODE

Seismograms can also be produced by a 2D time-stepping finite difference (FD) code for isotropic media (Manning, 2008; 2007). Finite difference elastic modeling will automatically generate direct P and S arrivals as well as all the refracted, reflected, and converted arrivals due to the boundaries in the velocity-density model. Because of stability issues related to FD modeling and the desire to have reasonable execution speed and grid array size, we have restricted the dominant frequencies in the synthetic seismograms to be 300 Hz or less. These are low compared to frequencies exceeding 500 Hz commonly observed for microseismic events associated with hydraulic fracturing projects.

Since it is a 2D code, the relative amplitudes and phases of the various arrivals will not be correct for microseismic source in 3D space, but the kinematics (i.e., arrival times) will be correct. For the direct P arrival, the *x* and *z* amplitudes will be correct in the 2D plane. To simulate the *x* and *y* amplitudes in 3D space, the P-wave *x* amplitudes from the 2D code are split by applying the direction cosines from the source to each receiver. This is a straightforward calculation, since for a horizontally-layered velocity model, the projection of the propagation vector between the source and receiver onto the *x*-*y* plane is a straight line.

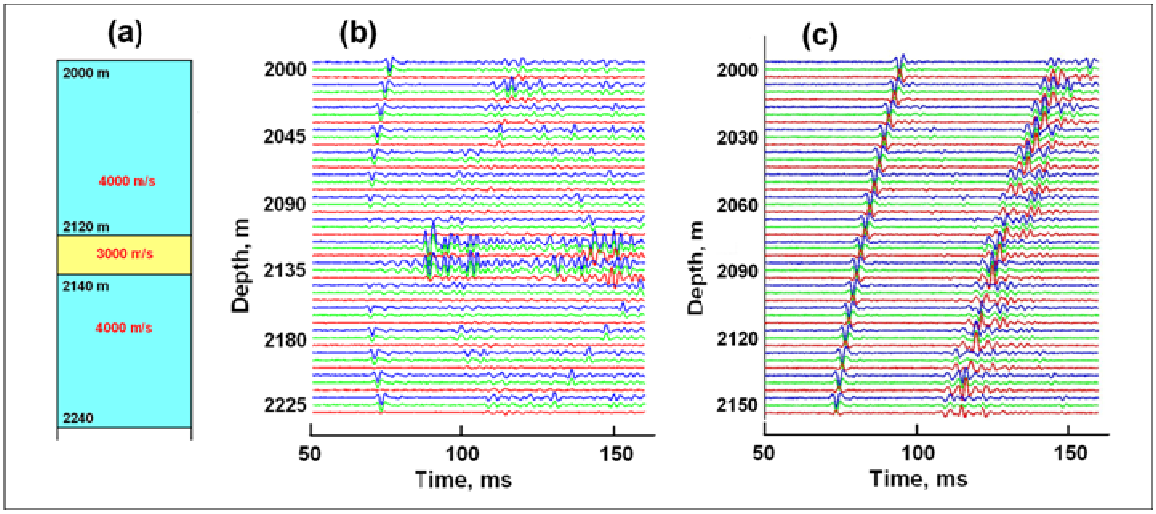

FIG. 6. (a) Velocity model for finite difference modeling of microseismograms; (b) Seismograms for an array of sixteen 3C geophones straddling the low-velocity zone; geophone spacing is 15 m. (c) Seismograms for an array entirely above the low-velocity zone; geophone spacing is 10 m.

Figure 6(a) shows a simple three-layer model for the finite difference calculations. Figures 6(b) and 6(c) displays two gathers of microseismic traces for a source in the 3000 m/s shale layer at a depth of 2135 m shooting into vertical arrays located 250 m horizontally from the source. The P-wave velocities of the layers are shown on the figure; the S-wave velocities are 2500 m/s, 1875 m/s, and 2500 m/s;

the relative densities are 2.7, 2.5, and 2.7. The resulting finite-difference seismograms in Figure 6(b) are rather complex, with guided waves, mode conversions, and grid boundary artifacts clearly visible. The FD code for computing synthetic seismograms is much slower than the ray tracing method.

NOISY MICROSEISMOGRAMS

Microseismic arrivals on real field-recorded traces are often obscured by random noise, power line harmonics, and vibrations from machinery such as downhole pumps. To simulate these effects and different signal-to-noise ratios (SNRs), we add various levels of Gaussian noise and 60 Hz harmonic interference to our synthetic traces. Figures 7(a) and 7(b) show how strong noise affects the quality of microseismic gathers. It would be a challenge to locate a reliable hypocenter using an automatic process and the data on Figure 7(b).

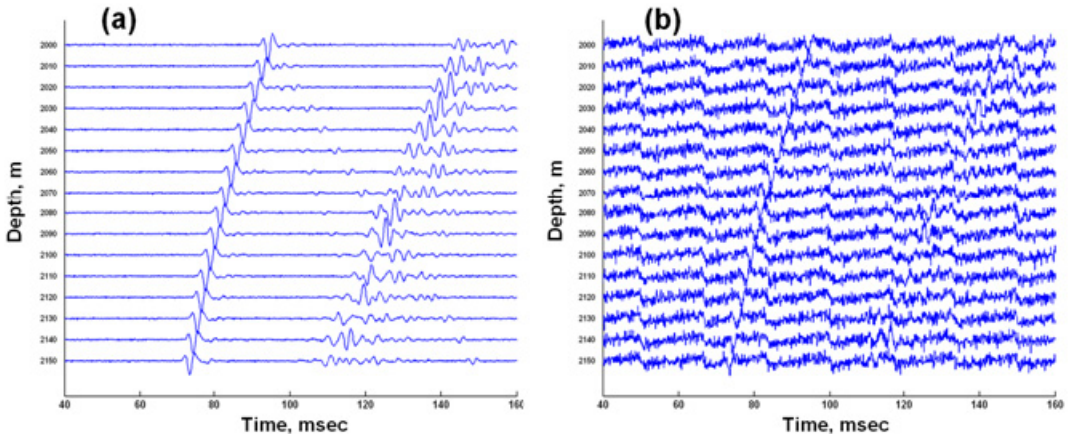

FIG. 7. (a) The FD x-component microseismograms with no noise. (b) The same seismograms after 60 HZ harmonic and Gaussian noise are added.

FILE STRUCTURE

The ray-traced arrival times give the correct absolute arrival times for the receivers. However, in recording real microseismograms, the arrival times recorded by a receiver array for each microseismic event are randomly delayed by an unknown time t_0. According, in order to provide a realistic simulation, we also apply a random delay for the data corresponding to a microseismic event.

Every synthetic microseismic file contains P and S arrivals for a single microseismic event. Each file contains 96 seismograms if the receiver array consists of 24 three-component geophones, or 48 seismograms if the array contains 16 geophones. Receivers can be placed anywhere on the surface of the layered earth, either randomly or in regular arrays. They may also be placed in deep or shallow wells with vertical, slanted, or horizontal sections. Datasets can be produced for receiver arrays in one, two, or three observation wells. Receiver spacings are set to 10 m, 25 m, or 50 m

The 3C seismograms are stored in SEG-2 format. The first three traces are the *x*, *y*, and *z* components for the first geophone, the next three traces are the *x*, *y*, and *z*

components for the second geophone, and so on. The x, y, and z coordinates of the geophones are recorded on the corresponding trace headers.

The sampling time is set to 0.25 ms, and each seismogram is 12,000 points or 3000 ms long. All arrivals on a particular file are delayed by a time t_0 randomly set to a value between 100 ms and 2975 ms, reflecting the fact that the actual event time is unknown.

CONCLUSION

Synthetic three–component microseismograms can be created using either ray-tracing or step-stepping finite difference modeling. The P and S velocity models used are discrete layers with horizontal boundaries. For the ray-tracing results, the modeled seismograms include only direct and head-wave arrivals, and the velocity model can include VTI or TTI anisotropy in the layers. The traces from FD modeling include converted as well as direct and head wave arrivals, but they do not include effects due to anisotropy. Gaussian and/or harmonic noise can be added to the synthetic microseismograms to simulate different signal-to-noise levels. The modeled data are stored in SEG2 format to conform to field-recorded data files.

The synthetic data are intended to be used for testing microseismic hypocenter location procedures within hypothetical but realistic geological structures and receiver array configurations. The synthetic seismograms described in this report are suitable only for testing hypocenter location methods that rely on observed arrival times and propagation directions at geophones. They do not contain any information that relate to source mechanisms.

ACKNOWLEDGEMENT

This research was supported by the NSERC and the industrial sponsors of CREWES.

REFERENCES

Byun, B.S., Corrigan, D., and Gaider, J.E., 1989. Anisotropic velocity analysis for lithology discrimination, Geophysics, **54**, 1566-1574.

Chambers, K., Brandsberg, S., Kendall, J.M., and Rueda, J., 2008. Testing the ability of surface arrays to locate microseismicity, 78th Ann. Int. Meeting, SEG, Expanded Abstracts, 1436-1439.

Han, L., Wong, J., and Bancroft, J.C., 2010. Back propagation analysis for hypocenter location, CREWES Research Report, this volume.

Kumar, D., Sen, M.K., and Ferguson, R.J., 2004. Traveltime calculation and prestack depth migration in tilted transversely isotropic media, Geophysics, **69**, 37-44.

Manning, P.M., 2008. Techniques to enhance the accuracy and efficiency of finite-difference modeling for the propagation of elastic waves, Ph.D. Thesis, University of Calgary.

Manning, P.M., 2008. Finite-difference elastic modeling in MATLAB, workbench version, CREWES Research Report, **20**, 24.1-24.10.

Wong, J., 2009. Microseismic hypocenter location using nonlinear optimization, CREWES Research Report, **21**, 73.1-73.14.

Wong, J., Han, L., and Bancroft, J.C., 2010. Microseismic hypocenter location using nonlinear optimization, 80th Ann. Int. Meeting, SEG, Expanded Abstracts, 2186-2190.